Dynamics of Gas Bubble Growth in Oil-Refrigerant Mixtures under Isothermal Depressurization

João Paulo Dias
jpdias@polo.ufsc.br
Department of Mechanical Engineering
Federal University of Santa Catarina
88040900 Florianópolis, SC, Brazil

Jader R. Barbosa Jr.
jrb@polo.ufsc.br
Department of Mechanical Engineering
Federal University of Santa Catarina
88040900 Florianópolis, SC, Brazil

Alvaro T. Prata
prata@polo.ufsc.br
Department of Mechanical Engineering
Federal University of Santa Catarina
88040900 Florianópolis, SC, Brazil

This paper proposes a numerical model to predict the growth of gaseous refrigerant bubbles in oil-refrigerant mixtures with high contents of oil subjected to isothermal depressurization. The model considers an Elementary Cell (EC) in which a spherical bubble is surrounded by a concentric and spherical liquid layer containing a finite amount of dissolved liquid refrigerant. The pressure reduction in the EC generates a concentration gradient at the bubble interface and the refrigerant is transported to the bubble by molecular diffusion. After a sufficiently long time, the concentration gradient in the liquid layer and the bubble internal pressure reach equilibrium and the bubble stops growing, having attained its stable radius. The equations of momentum and chemical species conservation for the liquid layer, and the material balance at the bubble interface are solved via a coupled finite difference procedure to determine the bubble internal pressure, the refrigerant radial concentration distribution and the bubble growth rate. Numerical results obtained for a mixture of ISO VG10 polyolester oil and refrigerant HFC-134a showed that the bubble growth dynamics depends on model parameters such as the initial bubble and liquid layer radii, the initial refrigerant concentration in the liquid layer, the initial pressure in the liquid phase, the decompression rate and the EC temperature. Despite its simplicity, the model demonstrated to be a potential tool for predicting bubble growth and foaming that may occur as a result of cavitation in oil-lubricated bearings and refrigerant degassing from the oil sump during compressor start-up.
Keywords: *refrigeration compressor, oil-refrigerant mixtures, bubble growth, numerical modeling*

Introduction

The interaction between the lubricant oil and the refrigerant is a key aspect in the determination of the refrigeration hermetic compressor performance and reliability. Its importance stems from the fact that the oil stored in the compressor sump is kept in direct contact with the gas inside the crankcase. The refrigerant usually has a significant solubility in the oil, which depends on pressure and temperature, and thermodynamic equilibrium between the phases is generally attained by means of refrigerant absorption and/or release from the mixture in some regions inside the compressor. Gas release (desorption) is caused primarily by pressure reduction during compressor start-up, but it is also caused by fluid friction as refrigerant-saturated lubricant flows through the compressor channels and gaps. As a result, small gas bubbles are formed which, in turn, change the bulk lubricant properties. If the pressure reduction is fast enough, bubble nucleation is so intense that foam can be formed (Becerra, 2003). It has been argued that cavitation and degassing phenomena can affect the compressor performance parameters such as power consumption and volumetric efficiency, and also provoke noise and wear (Grando et al., 2006a).

Gas evolution and foam formation in oil-refrigerant mixtures can affect the compressor tribological characteristics (Yanagisawa et al., 1991). Although the first studies concerning the lubrication of the compressor sliding parts neglected the presence of refrigerant dissolved in the oil (Prata et al., 2000; Rigola et al., 2003; Cho and Moon, 2005; Couto, 2006), they undoubtedly have set the foundations for the more recent class of lubrication models that considered the effect of a lubricant mixture composed of refrigerant and oil. Among these studies, Grando et al. (2006b) proposed simplified lubrication models for journal bearings considering the interaction between the oil and the refrigerant and the existence of a gas/liquid two-phase flow in the lubricant film. Grando et al. (2006a) solved the piston dynamics for small reciprocating compressors. Their results indicated an increase of friction losses followed by a reduction in load capacity due to the presence of gaseous refrigerant dispersed in the lubricant film.

The complex fluid flow behavior of oil-refrigerant mixtures imposes an additional difficulty to the development of more sophisticated lubrication models. Visual experiments of oil-rich mixtures flowing through long small diameter tubes carried out by Lacerda et al. (2000) and Castro et al. (2004) pointed out the existence of bubbly two-phase flow preceded by a significant region of metastable liquid flow. In these studies, after nucleation, as the pressure gradient departs from the constant value associated with single-phase flow and increases due to refrigerant outgassing, more bubbles are generated and become very closely spaced giving rise to a foamy structure. In the light of these findings, equilibrium models for oil-refrigerant two-phase flow were proposed by Grando and Prata (2003) and Dias and Gasche (2006), who modeled the homogeneous equilibrium two-phase bubbly and foam flow, and by Barbosa et al. (2004) and Castro et al. (2009) who correlated the two-phase frictional pressure drop. Without empirically-based corrections, homogeneous equilibrium models showed large discrepancies with respect to the experimental data of Lacerda et al. (2000) and Castro et al. (2004), indicating that a non-equilibrium analysis of oil-refrigerant two-phase flow is necessary.

Non-equilibrium models are based on the existence of pressure, temperature or chemical potential differences between the gas and the liquid phases. For dispersed systems such as two-phase bubbly and foam flows, non-equilibrium models generally also take into account nucleation and growth of individual gas bubbles in the liquid phase. These models have been widely employed to describe the growth of bubble clusters and foam growth in polymers and viscoelastic fluids (Amon and Denson, 1984; Arefmanesh and Advani, 1991; Arefmanesh et al., 1992; Joshi et al., 1998) and in magmatic melts (Proussevitch et al., 1993; Proussevitch and Sahagian, 1996).

Paper received 10 January 2011. Paper accepted 21 October 2011
Technical Editor: José Parise

In spite of the significant number of papers in related fields, the physical mechanisms that govern bubble growth in oil-refrigerant mixtures have never been studied from their first principles. This is, therefore, the main contribution of the present paper. Based on the works of Amon and Denson (1984) and Proussevitch et al. (1993), a numerical model to predict the growth of gas bubbles subjected to isothermal decompression is proposed, whereby the transient transport of refrigerant to the bubble is driven by molecular diffusion. The model considers an Elementary Cell (EC) formed by a spherical gas bubble surrounded by a concentric liquid layer with a finite amount of dissolved refrigerant. As the pressure reduces in the liquid layer, a concentration gradient at the expanding bubble interface induces a refrigerant mass flow into the bubble. After a sufficiently long period, the concentration gradient at the bubble interface vanishes, the bubble internal pressure reaches equilibrium and the bubble stops growing, having attained its final equilibrium radius. The equations of conservation of momentum and chemical species for the liquid layer are solved together with the bubble interfacial material balance via a coupled finite difference procedure to determine the bubble internal pressure, the refrigerant concentration distribution along the liquid layer and the bubble growth rate. It will be demonstrated quantitatively that, for a mixture of ISO VG10 polyol ester lubricant oil and refrigerant HFC-134a, the bubble growth process is characterized by three distinct periods. The first period is one of slow rate of growth (controlled by the effect of interfacial tension), the second period is one in which the bubble reaches its maximum radius (diffusion-controlled growth), and the third period is characterized by a vanishing concentration gradient in the liquid layer, when the bubble reaches its stable radius. In general terms, the numerical model results show that the bubble growth dynamics depends on the initial bubble and liquid layer radii, the initial pressure and refrigerant concentration in the liquid layer, the decompression rate and the elementary cell temperature.

Nomenclature

A_E = *coefficient in Eqs. (31)-(36)*
A_P = *coefficient in Eqs. (31)-(36)*
A_W = *coefficient in Eqs. (31)-(36)*
B = *coefficient in Eqs. (31)-(37)*
C = *coefficient in Eq. (33)*
D = *mass diffusivity of the refrigerant in the mixture, m² s^{-1}*
M = *mass, kg*
p = *pressure, Pa*
p_{sat} = *refrigerant vapor pressure, Pa*
r = *radial coordinate, m*
R = *bubble radius, m*
S = *liquid layer radius, m*
T = *temperature of the Elementary Cell, °C*
t = *time, s*
u_r = *liquid velocity in the radial direction, m s^{-1}*
w_r = *refrigerant mass concentration in the mixture*
w_{sat} = *refrigerant solubility in the mixture*
Y_0, = *dimensionless parameter in Eq. (27)*
Y_1, = *dimensionless parameter in Eq. (27)*
Y_2, = *dimensionless parameter in Eq. (27)*
Y_3, = *dimensionless parameter in Eq. (27)*
Y_4, = *dimensionless parameter in Eq. (27)*
y = *modified radial coordinate, m³*
y^* = *modified radial coordinate, m³*

Greek Symbols

β = *clustering parameter of the spatial grid*
φ = *potential function, m^{-3}*
μ = *dynamic viscosity, Pa s^{-1}*
ρ = *density, kg m³*
σ = *interfacial tension, N m^{-1}*
τ_{rr} = *component of the spherical stress tensor, Pa*
$\tau_{\theta\theta}$ = *component of the spherical stress tensor, Pa*
$\tau_{\phi\phi}$ = *component of the spherical stress tensor, Pa*
ζ = *auxiliary coordinate for the radial direction, m^{-3}*

Subscripts

b = *relative to the bubble*
F = *relative to the final (stable) bubble radius*
G = *gas phase*
j = *spatial grid index*
L = *liquid phase*
oil = *relative to the oil*
r = *relative to the refrigerant in the liquid layer*
0 = *relative to the initial instant*

Superscripts

$\wedge$ = *relative to the normalized variables*

Mathematical Modeling

Figure 1 shows a schematic diagram of the proposed physical model. It considers an EC in which a spherical bubble is surrounded by a concentric and spherical liquid layer with a finite amount of dissolved liquid refrigerant. At $t = 0$ the bubble and the liquid layer initial radii are R_0 and S_0, and the refrigerant concentration in the liquid layer is uniform ($w_{r,0}$). This initial condition is one of mechanical and chemical equilibrium between the gas and the liquid, which is at a pressure $p_{L,0}$. The bubble growth process is initiated when the pressure in the liquid layer is reduced according to a prescribed function $p_L(t)$. As the liquid pressure is reduced, the interfacial refrigerant concentration decreases and a refrigerant concentration gradient in the liquid layer drives the refrigerant flow into the bubble, increasing its size. At the same time, the liquid layer radius $S(t)$ is allowed to expand together with the bubble, since no constraint is imposed at the outer surface of the liquid layer. It is worth mentioning that local thermodynamic equilibrium is assumed at the liquid-gas interface, and that the interfacial solubility, w_{sat}, is calculated as a function of the EC temperature and of the bubble internal pressure $p_G(t)$. After a sufficiently long period ($t \rightarrow \infty$), a significant fraction of the total amount of refrigerant initially in the liquid layer is present in the form of gas inside the bubble, which eventually reaches its final (stable) radius, R_F, and its final internal pressure $p_{G,F}$.

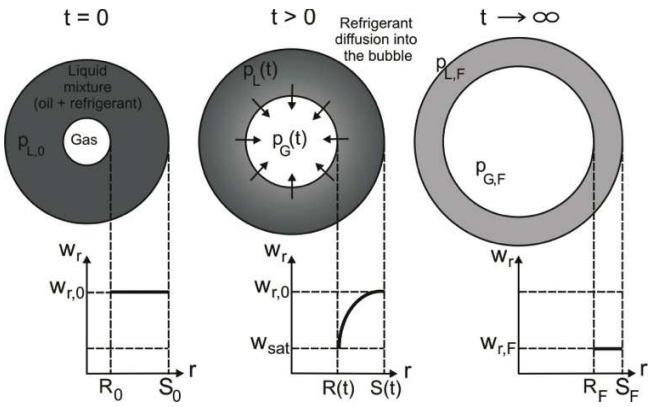

Figure 1. Schematic representation of the bubble growth dynamics in an oil-refrigerant mixture.

Simplifying Assumptions

The mathematical modeling is based on the following assumptions:

- The bubble and the liquid layer are perfectly spherical and the origin of the system of coordinates is located at the center of the bubble;
- The gas phase is composed only of refrigerant vapor (i.e., the vapor pressure of the oil is negligible) and the liquid phase behaves as an ideal mixture (Raoult's law);
- The fluids are Newtonian, with constant properties;
- Temperature gradients in the EC are negligible;
- The pressures in the bubble and in the liquid layer are uniform;
- The refrigerant mass fraction at the bubble interface is the saturation concentration (solubility) at the bubble pressure and EC temperature;
- The decompression rate imposed on the liquid phase is uniform.

Momentum Conservation in the Liquid Layer

The transient momentum transfer in the liquid layer in spherical coordinates, considering radial symmetry, is given by (Bird et al., 2002):

$$\rho_L\left(\frac{\partial u_r}{\partial t}+u_r\frac{\partial u_r}{\partial r}\right)=-\frac{\partial p}{\partial r}+\frac{1}{r^2}\frac{\partial}{\partial r}\left(r^2\tau_{rr}\right)-\frac{\left(\tau_{\theta\theta}+\tau_{\phi\phi}\right)}{r} \tag{1}$$

where ρ_L is the liquid phase density, u_r is the liquid velocity in the radial direction, p is the pressure, and τ_{rr}, $\tau_{\theta\theta}$ and $\tau_{\phi\phi}$ are the components of the spherical stress tensor given by

$$\tau_{rr}=2\mu_L\frac{\partial u_r}{\partial r} \tag{2a}$$

$$\tau_{\theta\theta}=\tau_{\phi\phi}=2\mu_L\frac{u_r}{r} \tag{2b}$$

where μ_L is the liquid phase dynamic viscosity.

A refrigerant material balance at the bubble interface gives (Brennen, 1995):

$$u_r r^2=R^2\dot{R} \tag{3}$$

where R and $\dot{R}$ are, respectively, the instantaneous bubble radius and its time derivative that represents the bubble growth rate. By substituting Eqs. (2) and (3) into Eq. (1), and taking advantage of the spherical symmetry of the problem ($\tau_{\theta\theta}$ = $\tau_{\phi\phi}$), the following relationship is obtained:

$$\rho_L\left(\frac{R^2\ddot{R}+2R\dot{R}^2}{r^2}-\frac{2R^4\dot{R}^2}{r^5}\right)=-\frac{\partial p}{\partial r}+\frac{\partial\tau_{rr}}{\partial r}+2\frac{\left(\tau_{rr}-\tau_{\phi\phi}\right)}{r} \tag{4}$$

where $\ddot{R}$ is the bubble growth acceleration, i.e., the second derivative of the bubble radius with respect to time. The liquid density is assumed constant and Eq. (4) can be integrated between the limits R and S (see Fig. 1) to give

$$\rho_L\left[\left(1-\frac{R}{S}\right)\left(R\ddot{R}+2\dot{R}^2\right)-\frac{1}{2}\dot{R}^2\left(\frac{R^4}{S^4}\right)\right]= \tag{5}$$
$$p(R)-\tau_{rr}(R)-p(S)+\tau_{rr}(S)+2\int_R^S\frac{\left(\tau_{rr}-\tau_{\phi\phi}\right)}{r}dr$$

The integral in Eq. (5) can be determined upon substitution of Eqs. (2) and (3), considering a uniform viscosity in the liquid layer. A change of variables is also introduced as follows:

$$2\int_R^S\frac{\left(\tau_{rr}-\tau_{\phi\phi}\right)}{r}dr=-12R^2\dot{R}\int_R^S\frac{\mu_L}{r^4}dr= \tag{6}$$
$$-4R^2\dot{R}\int_{\zeta(R)}^{\zeta(S)}\mu_L(\zeta)\,d\zeta$$

where ζ is an auxiliary coordinate defined by

$$\zeta=\frac{1}{r^3};\ \zeta(R)=\frac{1}{R^3};\ \zeta(S)=\frac{1}{S^3} \tag{7}$$

Also, the normal stresses at the two ends of the radial domain can be expressed as (Street, 1971):

$$p(R)-\tau_{rr}(R)=p_G-\frac{2\sigma}{R} \tag{8a}$$

$$p(S)-\tau_{rr}(S)=p_L \tag{8b}$$

where σ is the interfacial tension between the liquid mixture and the gaseous refrigerant. Finally, the incorporation of Eqs. (6)-(8) into Eq. (5) results in

$$\underbrace{p_G-p_L}_{\text{Pressure difference}}=\underbrace{\frac{2\sigma}{R}}_{\text{Interfacial tension}}\underbrace{-4R^2\dot{R}\int_{\zeta(R)}^{\zeta(S)}\mu_L(\zeta)\,d\zeta}_{\text{Viscous forces}}+ \tag{9}$$
$$\underbrace{\rho_L\left[\left(1-\frac{R}{S}\right)\left(R\ddot{R}+2\dot{R}^2\right)-\frac{1}{2}\dot{R}^2\left(\frac{R^4}{S^4}\right)\right]}_{\text{Inertia forces}}$$

The terms in Eq. (9) represent the various forces acting on the bubble during the growth process. The term on the left hand side is the driving force for bubble growth represented by the pressure difference between the gas inside the bubble and the liquid phase, while those on the right are the opposing forces, i.e, the resistance caused by the interfacial tension, the liquid viscous forces due to the interface motion and the resistance due the inertia of the liquid layer.

Chemical Species Conservation in the Liquid Layer

The refrigerant concentration profile in the liquid layer is calculated solving the chemical species conservation equation in spherical coordinates (Bird et al., 2002). Using Eq. (3) for the radial velocity of the liquid, the species mass balance can be written as:

$$\frac{\partial w_r}{\partial t} + \dot{R}\frac{R^2}{r^2}\frac{\partial w_r}{\partial r} = \frac{1}{r^2}\frac{\partial}{\partial r}\left(\rho_L D r^2 \frac{\partial w_r}{\partial r}\right) \tag{10}$$

where $w_r(r,t)$ is the refrigerant mass fraction profile and D is the mass diffusivity of the refrigerant in the liquid mixture, defined in terms of Fick's law (see Appendix). Equation (10) requires initial and boundary conditions defined as

$$w_r(r,0) = w_{r,0} \tag{11a}$$

$$\left.\frac{\partial w_r}{\partial r}\right|_{r=S} = 0 \tag{11b}$$

$$w_r(R,t) = w_{sat}(p_G, T) \tag{11c}$$

The three boundary conditions specified in Eqs. (11) refer, in this order, to (a) the uniform refrigerant concentration in the liquid layer at $t = 0$; (b) the absence of mass flux through the liquid layer external surface, and (c) that the liquid-vapor interface is at local thermodynamic equilibrium at the bubble internal pressure p_G and EC temperature T.

The geometry of the problem allows the following coordinate transformations:

$$y = r^3 - R^3(t) \tag{12a}$$

$$\frac{\partial \varphi}{\partial t} = w_r - w_{r,0} \tag{12b}$$

where y is a modified radial coordinate that takes into account the movement of bubble interface and $\varphi(y,t)$ is a potential function introduced to facilitate the solution of the mathematical model during the initial instants of bubble growth, due to the large concentration gradients at the vicinity of the interface (Amon and Denson, 1984). Substituting Eq. (12) into Eqs. (10) and (11) gives

$$\frac{\partial \varphi}{\partial t} = 9D\left(y + R^3\right)^{4/3}\frac{\partial^2 \varphi}{\partial y^2} \tag{13}$$

$$\varphi(y,0) = 0 \tag{14a}$$

$$\varphi(S^3 - R^3, t) = 0 \tag{14b}$$

$$\left.\frac{\partial \varphi}{\partial y}\right|_{y=0} = w_{sat} - w_{r,0} \tag{14c}$$

Bubble Material Balance

For a spherical bubble, the material balance results in

$$\frac{d}{dt}\left(R^3 \rho_G\right) = 3R^2\left(\rho_L D\frac{\partial w_r}{\partial r}\right)_{r=R} \tag{15}$$

After expanding the left hand side of Eq. (15) and applying the transformations of Eq. (12), the bubble growth rate equation becomes

$$\dot{R} = \frac{dR}{dt} = \frac{3R^2}{\rho_G}\left(\rho_L D\frac{\partial^2 \varphi}{\partial y^2}\right)_{y=0} - \frac{R}{3\rho_G}\frac{d}{dt}\left(\rho_G\right) \tag{16}$$

Closure Relationships

Equations (9), (13), (14) and (16) are the governing equations of the problem, which allow the calculation of the gas pressure inside the bubble, the refrigerant concentration profile in the liquid layer and the bubble growth rate as a function of time. However, some additional relationships are needed to provide closure for the model. These are as follows:

Initial bubble radius: due to the interfacial force acting on the bubble at the first instant of growth, a minimum initial radius must be defined. This minimum initial radius can be expressed in terms of the refrigerant vapor pressure, p_{sat}, at the EC temperature by the Young-Laplace relationship as follows (Carey, 1992):

$$R_0 > \frac{2\sigma}{p_{sat}(T) - p_{L,0}} \tag{17}$$

Final bubble radius: Proussevitch et al. (1993) suggested the use of a total refrigerant material balance between the initial and final instants of bubble growth to estimate R ($t \to \infty$) in terms of the liquid and gas phase densities, ρ_L and ρ_G:

$$\left(\rho_G R^3\right)_{t\to\infty} - \left(\rho_G R^3\right)_{t=0} = \left(S_0^3 - R_0^3\right)\left[(\rho_L w_r)_{t=0} - (\rho_L w_{sat})_{t\to\infty}\right] \tag{18}$$

Instantaneous liquid layer radius: as the EC is free to expand, the liquid layer radius can be calculated solving the following integral relationship for the instantaneous mass of liquid in the liquid layer, $M_L(t)$:

$$M_L(t) = 4\pi\int_{R(t)}^{S(t)} \rho_L(r,t)\, r^2\, dr \tag{19}$$

Numerical Solution Procedure

A convenient way to solve the coupled non-linear system formed by Eqs. (9), (13), (14) and (16) involves the normalization of the variables in order to simplify the numerical solution. Thus, the normalized governing equations are given by

$$\hat{p}_G - \hat{p}_L = \frac{Y_3\hat{\sigma}}{\hat{R}} + Y_1 Y_4 \hat{R}^2\dot{\hat{R}}\int_0^1 \frac{\hat{\mu}_L}{\left(\hat{y} + Y_1\hat{R}^3\right)}d\hat{y} + \hat{\rho}\left\{\left(1 - Y_0\frac{\hat{R}}{\hat{S}}\right)\left(Y_2\dot{\hat{R}}\hat{R} + 2Y_2\dot{\hat{R}}^2\right) - \frac{1}{2}Y_2\dot{\hat{R}}^2\left[1 - \left(Y_0\frac{\hat{R}}{\hat{S}}\right)^4\right]\right\} \tag{20}$$

$$\frac{\partial \hat{\varphi}}{\partial \hat{t}} = 9\hat{D}Y_1^{2/3}\left(\hat{y} + Y_1\hat{R}^3\right)^{4/3}\frac{\partial^2 \hat{\varphi}}{\partial \hat{y}^2} \tag{21}$$

$$\hat{\varphi}(\hat{y},0) = 0 \tag{22a}$$

$$\varphi(1,\hat{t}) = 0 \tag{22b}$$

$$\left.\frac{\partial\hat{\varphi}}{\partial\hat{y}}\right|_{\hat{y}=0} = w_{sat} - w_{r,0} \tag{22c}$$

$$\hat{\dot{R}} = \frac{d\hat{R}}{d\hat{t}} = \frac{3\hat{R}^2}{\hat{\rho}_G} Y_1 \left(\hat{\rho}_L \hat{D} \frac{\partial^2 \hat{\varphi}}{\partial \hat{y}^2} \right)_{\hat{y}=0} - \frac{\hat{R}}{3\hat{\rho}_G} \frac{d\hat{\rho}_G}{d\hat{t}} \tag{23}$$

where the normalized parameters are defined as

$$\hat{S} = \frac{S}{S_0};\ \hat{R} = \frac{R}{R_0};\ \hat{y} = \frac{y}{S_0^3 - R_0^3};\ \hat{\varphi} = \frac{\varphi}{S_0^3 - R_0^3} \tag{24}$$

$$\hat{t} = t\frac{D_0}{R_0^2};\ \hat{\dot{R}} = \dot{R}\frac{R_0}{D_0};\ \hat{\ddot{R}} = \ddot{R}\frac{R_0^3}{D_0^2} \tag{25}$$

$$\hat{p} = \frac{p}{p_{L,0}};\ \hat{D} = \frac{D}{D_0};\ \hat{\rho} = \frac{\rho}{\rho_{G,0}};\ \hat{\mu}_L = \frac{\mu_L}{\mu_{L,0}};\ \hat{\sigma} = \frac{\sigma}{\sigma_0} \tag{26}$$

$$Y_0 = \frac{R_0}{S_0};\ Y_1 = \frac{R_0^3}{S_0^3 - R_0^3};\ Y_2 = \frac{\rho_{G,0}}{p_{L,0}} \left(\frac{D_0}{R_0} \right)^2;$$

$$Y_3 = \frac{2\sigma_0}{R_0 p_{L,0}}\ Y_4 = \frac{4\mu_{L,0} D_0}{p_{L,0} R_0^2} \tag{27}$$

where the subscript "0" denotes the initial condition. For the solution of Eq. (21), with the boundary conditions presented in Eq. (22), a 1-D finite difference-based procedure was used according to the gridding scheme presented in Fig. 2.

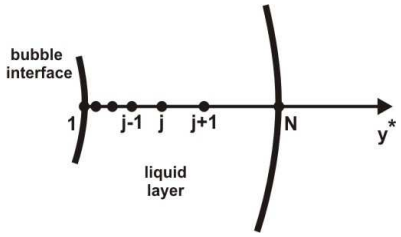

Figure 2. Finite difference-based gridding scheme in the liquid layer.

In order to accelerate convergence, an additional coordinate transformation (Anderson et al., 1984) is used to refine the computational grid in the region near the bubble interface. The transformation is defined as follows (Proussevitch et al., 1993):

$$\hat{y}(y^*) = \beta + 1 - (\beta - 1) \left(\frac{\beta+1}{\beta-1} \right)^{1-y^*} \left[1 + \left(\frac{\beta+1}{\beta-1} \right)^{1-y^*} \right]^{-1} \tag{28}$$

$$\frac{\partial\hat{\varphi}}{\partial\hat{y}} = \frac{\partial\hat{\varphi}}{\partial y^*} \frac{dy^*}{d\hat{y}} \tag{29a}$$

$$\frac{\partial^2\hat{\varphi}}{\partial\hat{y}^2} = \frac{\partial\hat{\varphi}}{\partial y^*} \frac{d^2 y^*}{d\hat{y}^2} + \frac{\partial^2\hat{\varphi}}{\partial y^{*2}} \left(\frac{dy^*}{d\hat{y}} \right)^2 \tag{29b}$$

$$\frac{dy^*}{d\hat{y}} = \frac{2\beta}{\left[\beta^2 - \left(1 - \hat{y} \right)^2 \right] \ln\left(\frac{\beta+1}{\beta-1} \right)} \tag{30a}$$

$$\frac{d^2 y^*}{d\hat{y}^2} = \frac{4\beta\left(\hat{y} - 1 \right)}{\left[\beta^2 - \left(1 - \hat{y} \right)^2 \right]^2 \ln\left(\frac{\beta+1}{\beta-1} \right)} \tag{30b}$$

in which $1 < \beta < \infty$ is a clustering parameter. The gridding near the interface becomes finer as this parameter approaches unity. Therefore, the linear system of N algebraic equations assumes the following form for each one of N points of the domain inside the liquid layer,

$$A_W \hat{\varphi}_{j-1} + A_P \hat{\varphi}_j + A_E \hat{\varphi}_{j+1} = B \tag{31}$$

where for the intermediate points ($1 < j < N$),

$$A_P = \frac{\left(y_j^* - y_{j-1}^* \right)^2}{C_j \Delta\hat{t}} + 2\frac{dy^*}{d\hat{y}} \tag{32a}$$

$$A_E = -\frac{\left(y_j^* - y_{j-1}^* \right)^2}{2} \frac{d^2 y^*}{d\hat{y}^2} - \frac{dy^*}{d\hat{y}} \tag{32b}$$

$$A_W = \frac{\left(y_j^* - y_{j-1}^* \right)^2}{2} \frac{d^2 y^*}{d\hat{y}^2} - \frac{dy^*}{d\hat{y}} \tag{32c}$$

$$B = \frac{\left(y_j^* - y_{j-1}^* \right)^2 \varphi_j^o}{C_j \Delta\hat{t}} \tag{33a}$$

$$C_j = 9 Y_1^{2/3} \left[\hat{y}\left(y^* \right) + Y_1 \hat{R}^3 \right]^{4/3} \tag{33b}$$

and for the boundary nodal points (1 and N),

$$A_{P,1} = -1;\quad A_{E,1} = 1;\quad A_{W,1} = 0 \tag{34}$$

$$B_1 = y_1^* (w_{sat} - w_{r,0}) \left(\frac{dy^*}{d\hat{y}} \right)^{-1} \tag{35}$$

$$A_{P,N} = 1;\quad A_{E,N} = 0;\quad A_{W,1} = 0 \tag{36}$$

$$B_N = 0 \tag{37}$$

The model considered an oil-refrigerant mixture composed of polyol ester oil (ISO VG10) and refrigerant HFC-134a. The relationships used to calculate thermophysical properties of the mixture are listed in the Appendix. The thermophysical properties of the pure oil and of the pure refrigerant were obtained from Dias and Gasche (2006) and McLinden et al. (1998), respectively. A flowchart of the numerical procedure is shown in Fig. 3.

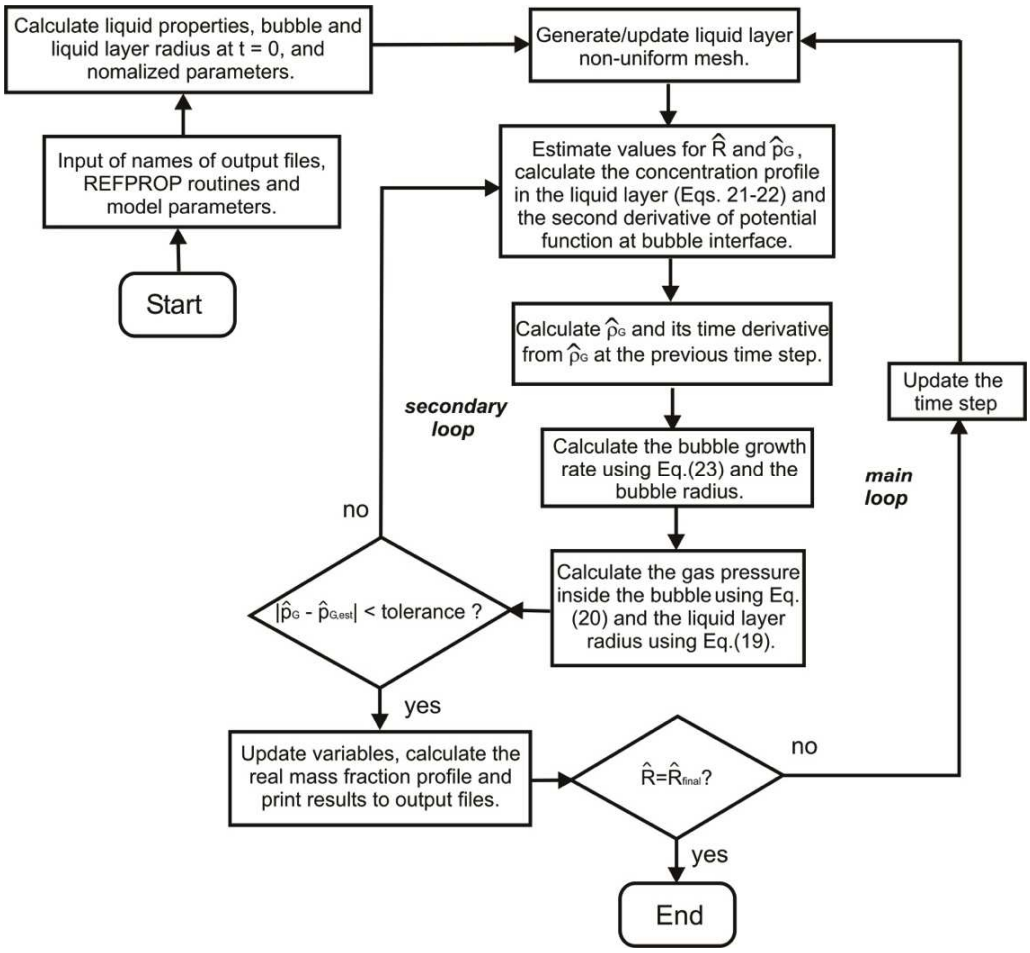

Figure 3. Flowchart of the numerical procedure for the solution of the bubble growth in oil-refrigerant mixtures.

Results and Discussion

A total number of 24 numerical simulations were executed to analyze the model response under different bubble growth conditions. Table 1 shows all cases simulated in the present work, and lists the main input and output parameters of the model. All numerical results were obtained for a spatial computational grid with 51 nodes in the liquid layer region and a time step of 10 μs. These were observed to be the minimum values that produced numerical results independent from the number of discrete points of time and spatial grids. Tolerances for the secondary and main loops were 10^{-6} and 99.9% of the calculated bubble final radius, respectively.

In order to verify the validity of the results, Table 1 presents the material balance error represented in terms of the relative difference between the bubble mass gain and the refrigerant depletion in the liquid layer during the whole growth period. Mathematically, this error can be calculated as

$$Err[\%] = 100\left|\frac{\Delta M_b - \Delta M_{r,L}}{\Delta M_b}\right| \tag{38}$$

where ΔM_b and $\Delta M_{r,L}$ are the bubble mass variation and the refrigerant mass variation in the liquid layer, respectively, given by

$$\Delta M_b = \frac{4}{3}\pi\left(\rho_{G,0}R_0^3 - \rho_{G,F}R_F^3\right) \tag{39}$$

$$\Delta M_{r,L} = \frac{4}{3}\pi\left[w_{r,0}\rho_{L,0}\left(S_0^3 - R_0^3\right) - w_{r,F}\rho_{L,F}\left(S_F^3 - R_F^3\right)\right] \tag{40}$$

where Eqs. (39) and (40) require knowledge of the parameters associated with the size of the bubble and of the liquid layer regions and refrigerant content at both the initial and final instants. As can be seen in Table 1, the majority of the simulations presented relative errors smaller than 1%. Also, the error tends to increase for cases where smaller quantities of refrigerant are transferred to the bubble, i.e., when both the initial thickness and the initial refrigerant mass concentration of the liquid layer are too small.

Figure 4 shows the behavior of the bubble and liquid layer radii for Simulation 1. The model computes the liquid layer growth due to bubble expansion (depressurization). The results show that the bubble growth process is characterized by three distinct periods

Table 1. Main parameters and results obtained with the mathematical model.

Simulation	**Parameters (Input)**						**Results (Output)**			
	S_0 [mm]	R_0 [mm]	$p_{L,0}$ [kPa]	dp_L/dt [kPa/s]	T [^{o}C]	$w_{r,0}$ [%]	t_F [s]	R_F [mm]	S_F [mm]	Material balance error [%]
1	1.00	10^{-2}	100.0	-100.0	60.0	5.0	1.65	4.99	5.17	0.41
2	1.00	10^{-2}	90.0	-100.0	80.0	1.0	3.96	3.70	3.79	0.15
3	1.00	9.5×10^{-2}	90.0	-100.0	80.0	1.0	3.84	3.70	3.79	0.15
4	1.00	0.5	90.0	-100.0	80.0	1.0	3.65	3.61	3.72	0.23
5	1.00	0.9	90.0	-100.0	80.0	1.0	1.39	3.06	3.24	0.96
6	0.10	5.0×10^{-3}	100.0	-100.0	80.0	5.0	0.90	0.52	0.85	6.19
7	0.50	5.0×10^{-3}	100.0	-100.0	80.0	5.0	1.06	2.56	2.88	0.96
8	1.50	5.0×10^{-3}	100.0	-100.0	80.0	5.0	1.95	7.54	7.79	0.17
9	3.00	5.0×10^{-3}	100.0	-100.0	80.0	5.0	5.40	15.00	15.40	0.07
10	1.00	10^{-2}	90.0	-100.0	80.0	0.95	3.84	3.63	3.72	1.98
11	1.00	10^{-2}	90.0	-100.0	80.0	3.0	1.49	5.45	5.55	0.17
12	1.00	10^{-2}	90.0	-100.0	80.0	5.0	1.17	6.54	6.67	0.21
13	1.00	10^{-2}	90.0	-100.0	80.0	10.0	0.97	8.37	8.56	0.28
14	1.00	10^{-2}	10.0	-100.0	80.0	5.0	0.46	6.55	6.63	0.16
15	1.00	10^{-2}	100.0	-100.0	80.0	5.0	1.27	6.54	6.67	0.21
16	1.00	10^{-2}	250.0	-100.0	80.0	5.0	2.78	6.55	6.69	0.24
17	1.00	10^{-2}	400.0	-100.0	80.0	5.0	4.25	6.55	6.70	0.24
18	1.00	10^{-2}	100.0	-10.0	80.0	5.0	12.7	5.07	5.48	0.66
19	1.00	10^{-2}	100.0	-50.0	80.0	5.0	2.55	5.05	5.34	0.39
20	1.00	10^{-2}	100.0	-100.0	80.0	5.0	1.66	5.10	5.30	0.31
21	1.00	10^{-2}	100.0	-100.0	25.0	5.0	7.50	4.75	4.91	0.99
22	1.00	10^{-2}	100.0	-100.0	35.0	5.0	5.31	4.83	4.99	0.67
23	1.00	10^{-2}	100.0	-100.0	50.0	5.0	3.48	4.93	5.10	0.48
24	1.00	10^{-2}	100.0	-100.0	100.0	5.0	1.55	5.21	5.43	0.27

(Proussevitch et al., 1993). The first period is marked by a slow growth of the bubble and liquid layer radii, which is generally attributed to the high interfacial tension. In this period, growth is controlled by the interfacial tension and normal viscous stresses that offer a resistance to growth associated with displacing the body of liquid around the bubble. At 1.2 seconds following this initial period, the growth rate increases up to a point of maximum. This marks the second period of bubble growth, which is called here the effective growth period. This period is controlled by mass diffusion, as the excess dissolved refrigerant that existed in the first period is transported into the bubble. The bubble and liquid layer reach stable radii in the third period, when the concentration gradient in the liquid layer vanishes. At the end of the process, the bubble and the liquid layer reach, respectively, around 500 and 5 times their initial radii.

An analysis of the forces that affect the bubble growth for Simulation 1 is presented in Fig. 5, which shows the force caused by the pressure difference between the gas and liquid phases (the growth driving force) and the forces resulting from interfacial tension, viscous stresses and liquid inertia. All forces are depicted in normalized form, as presented in Eq. (20), to facilitate the analysis. As can be verified for this case, the main opposing force for bubble growth is generated by the interfacial tension; almost no difference is observed between the pressure difference and interfacial tension curves at any given instant. Thus, the small resultant force associated with the pressure difference, interfacial tension and viscous forces is the net force that drives the bubble growth. This small difference is due to the small initial radius chosen for the bubble, which, in turn, determines the slow growth rate period pointed out previously.

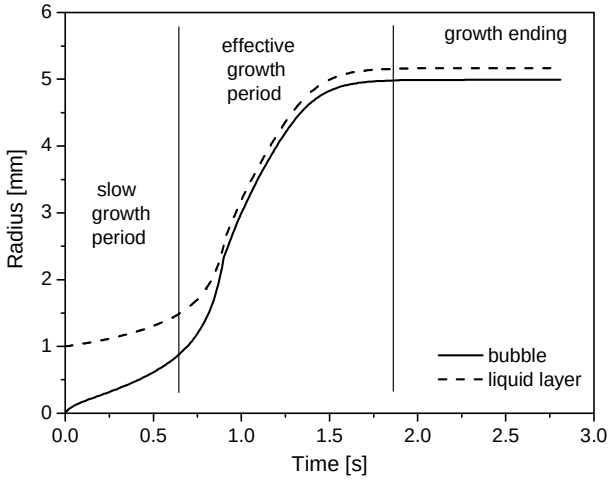

Figure 4. Bubble and liquid layer growth behavior for Simulation 1.

Figure 6 analyzes the refrigerant transport by diffusion in the liquid layer by comparing the refrigerant concentration profiles in liquid layer at different instants for Simulation 1. Each instant is indicated in the figure as a fraction of the time necessary for the bubble to reach 99% of its final radius t_F, and the liquid layer thickness is normalized to facilitate the comparison among the different instants considered. Starting from a uniform refrigerant concentration at $t = 0$, the first few instants after diffusion starts (until around 30% of t_F) indicate that almost no change takes place in the

concentration profile far from the bubble interface. This period of time is also characterized by high concentration gradients near the interface. Then, as the bubble growth speed increases, refrigerant solubility at the interface decreases due to the decrease in gas pressure, and the gradient at the interface becomes smoother as the refrigerant in the liquid layer is transported towards the interface, thus reducing the total amount of refrigerant available in the liquid layer. Finally, after 1.65 s, when the bubble reaches 99.9% of its final radius, the interfacial concentration reaches equilibrium with the remaining liquid layer and the bubble stops growing.

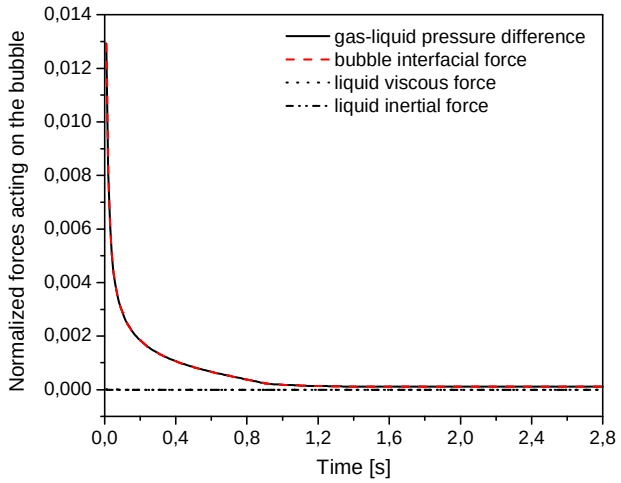

Figure 5. Forces acting on the bubble during the growth period for Simulation 1.

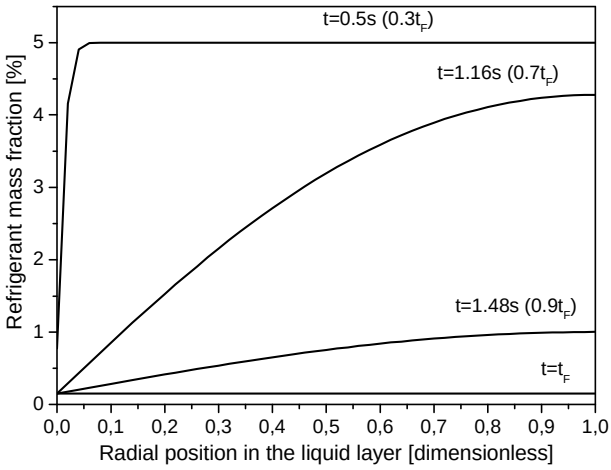

Figure 6. Refrigerant mass fraction distribution along the liquid layer at different instants for Simulation 1.

The terms on the right side of Eq. (16) represent the two main mechanisms that govern bubble growth. The first term represents the growth induced by refrigerant molecular diffusion from the liquid layer towards the bubble, while the second term is the portion of the growth due to expansion of the gas inside the bubble as the pressure in the liquid layer decreases. The effect of both terms on total bubble growth rate along the time for Simulation 1 is shown in Fig. 7. Right after the beginning of the bubble growth process, the growth rate is governed exclusively by bubble expansion, which decreases as the interfacial force acting on the bubble remains large. This behavior is consistent with the period of slow growth described earlier in Fig. 4. When the bubble reaches a sufficiently large size to overcome the opposing interfacial force, both gas expansion and refrigerant molecular diffusion effects increase rapidly and contribute equally to the growth rate that reaches its maximum value. Then, a sudden decrease of the molecular diffusion growth rate takes place indicating that the amount of excess refrigerant present in the liquid layer has extinguished, and the growth process is again governed by gas expansion effect, which vanishes slowly as the bubble reaches its final size.

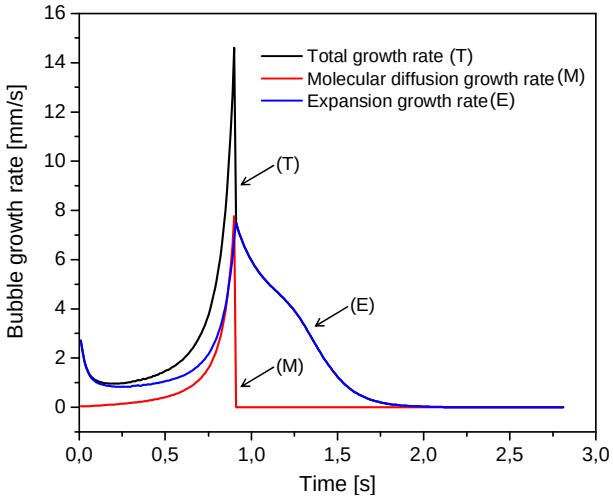

Figure 7. Bubble growth rates along the time for Simulation 1.

Figure 8 shows the effect of variation of the initial bubble radius on the bubble growth behavior. It can be observed that the smaller the initial radius, the longer the slow growth period will be due to the large interfacial force at the initial instants of bubble growth. Additionally, there is almost no difference between the bubble growth curves when the initial bubble radii were smaller than 9.5×10^{-2} mm (Simulations 2 and 3). It is believed that this has to do with the fact that for these initial bubble diameters, the interfacial tension force is still quite large and, because the sizes of the bubbles are small, the amount of volatile material (refrigerant) in the liquid layer is very similar in both cases. Nevertheless, when the initial radius was set to 0.5 and 0.9 mm in Simulations 4 and 5, respectively, the final bubble radius and the time required to reach the stable size decreased because of the reduction in the liquid layer thickness that contained smaller amounts of liquid and volatile material.

The result presented in Fig. 9 evaluates the influence of the liquid layer initial radius on the bubble growth behavior for Simulations 6-9. It can be noticed that, although the initial concentration of refrigerant was the same for all cases simulated (5% wt.), the liquid layer radius limits the final radius reached by the bubble. This is a consequence of the smaller amount of refrigerant initially in the liquid layer for the smallest liquid layer radii. Moreover, the influence of interfacial tension was more important as the liquid layer radius was decreased. This is clearly noticed in the result for Simulation 6, where bubble growth is slow for most of the time, until the stable radius is reached more abruptly.

The effect of the initial refrigerant concentration is shown in Fig. 10. A preliminary analysis of this result leads to the conclusion that the higher the amount of refrigerant dissolved in the liquid layer, initially, the higher the bubble final radius. However, the time required for a bubble to reach its final radius is smaller as the initial refrigerant concentration increases. This seems counter-intuitive considering the idea that a larger amount of dissolved refrigerant should take longer to flow into the bubble, thus also taking more

time for the final radius to be reached than in the case with less dissolved refrigerant. However, the cases with higher initial refrigerant concentrations presented the steepest slopes of the bubble radius variation in the first 0.8 s. This occurs due to the high concentration gradients generated in the liquid layer when the total amount of refrigerant dissolved in the liquid increases. Under these conditions, the solubility at the interface is the same for all simulations, and the net result is a higher mass flow rate of refrigerant into the bubble for the simulations with a higher initial refrigerant concentration in the liquid layer.

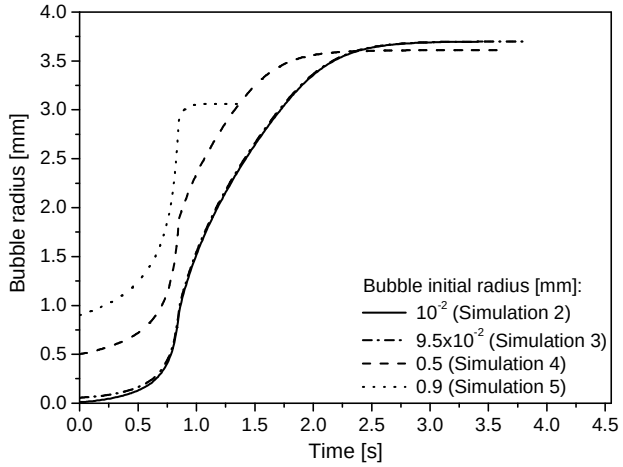

Figure 8. Influence of the initial bubble radius on the bubble growth behavior.

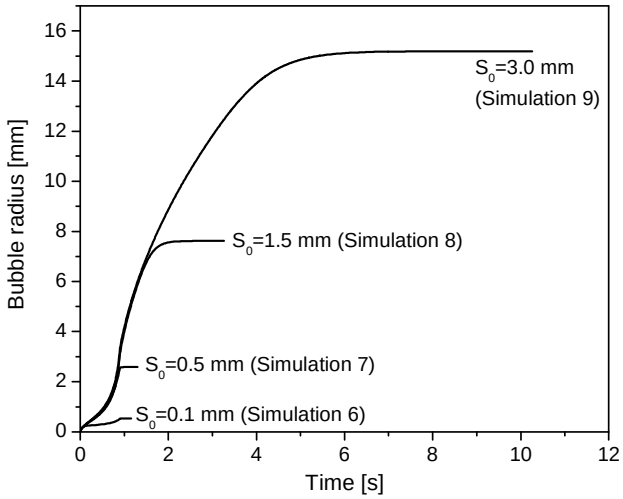

Figure 9. Influence of the initial liquid layer radius on the bubble growth behavior.

Figure 11 presents an evaluation of the initial liquid phase pressure on the bubble growth behavior for Simulations 14-17. The main characteristic of these results is the fact that the duration of the first period increases with the initial pressure. This is so because the solubility is directly proportional to the pressure. Hence, an increase in the initial liquid pressure reduces the refrigerant supersaturation degree in the liquid layer. So, the observed behavior is a consequence of the reduction of the concentration gradient near the interface, which decreases the refrigerant mass flow rate into the bubble. It is also worth mentioning that the bubble final radius was the same for all simulations since the initial refrigerant concentration and the final pressure in the liquid layer were also kept the same for all simulations.

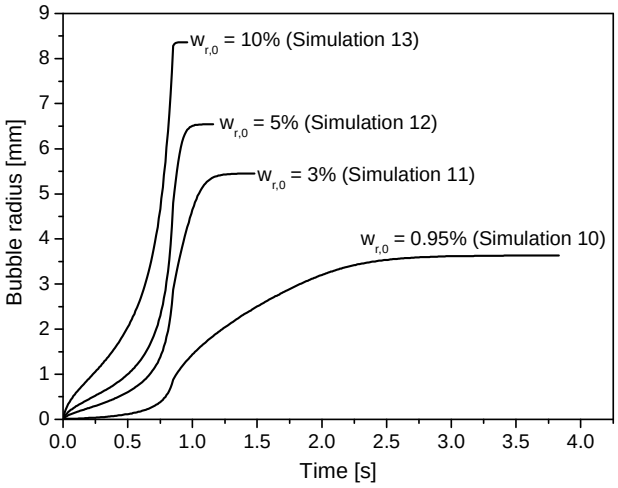

Figure 10. Influence of the initial refrigerant concentration in the liquid layer on the bubble growth behavior.

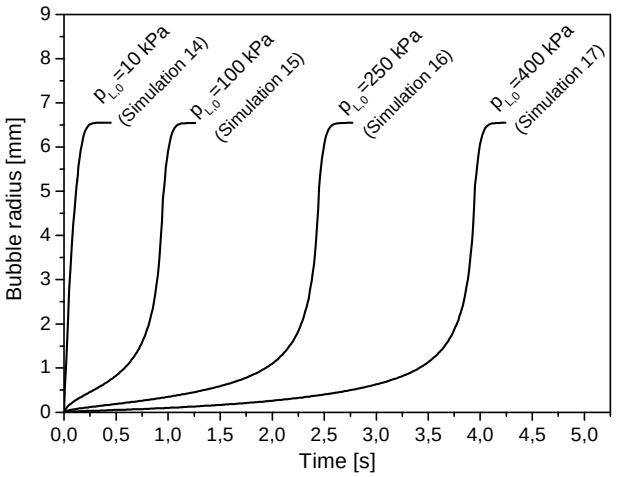

Figure 11. Influence of the initial pressure in the liquid phase on the bubble growth behavior.

Differently from previous works that studied isothermal bubble growth in polymer solutions and volcanic magma (Amon and Denson, 1984; Proussevitch et al., 1993), in the present paper, a finite decompression rate was assumed in the liquid phase from both prescribed initial and final pressures in the liquid layer. This is a convenient approach to deal with oil-refrigerant mixtures, since this model can be coupled to existing macroscopic models aiming at a more complete characterization of non-equilibrium flows of oil-refrigerant mixtures. Figure 12 depicts the behavior of bubble growth for Simulations 18-20 considering different liquid phase decompression rates. The graphs indicate that, as the pressure in the liquid layer is reduced more slowly, more time is needed for the bubble to reach its final radius. This behavior occurs because bubble growth driven by gas expansion becomes slower than that due to interfacial refrigerant mass flow rate as the decompression rate decreases.

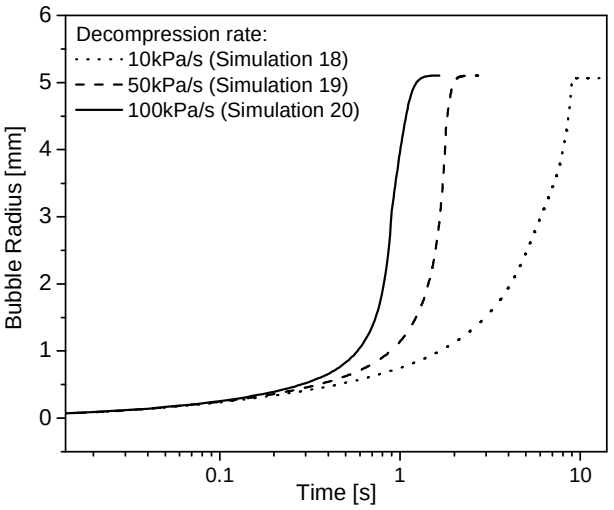

Figure 12. Influence of the decompression rate on the bubble growth behavior.

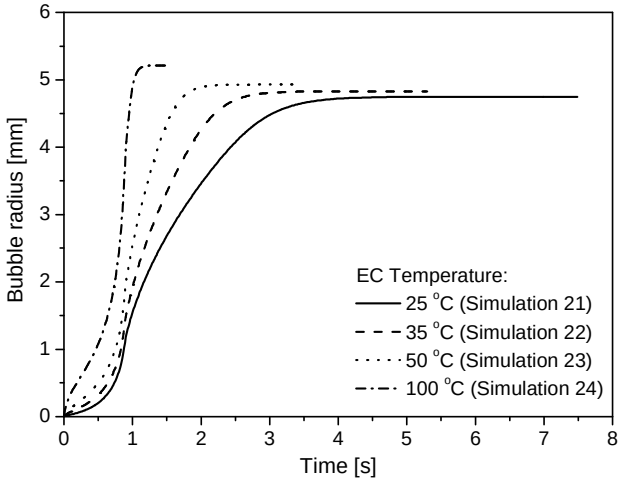

Figure 13. Influence of the elementary cell temperature on the bubble growth behavior.

Figure 13 presents an evaluation of the effect of the EC temperature on the bubble radius behavior as a function of time for Simulations 21-24. An increase of the EC temperature reduces the dynamic viscosity and increases the mass diffusivity of the mixture so that the combination of both effects leads to faster bubble growth rates since, as the EC temperature increases, viscous forces that resist to bubble growth are smaller and, at the same time, larger mass diffusivities contribute to improving refrigerant mobility inside the liquid layer. Another observation regarding the effect of EC temperature on bubble dynamics is the different final radius reached in each simulation. This occurs because the equilibrium concentration at the interface is inversely proportional to the EC temperature, which gives rise to a higher supersaturation degree in the liquid layer. So, a larger amount of refrigerant can flow into the bubble making its final radius larger.

Conclusions

This paper presented a transient model for a single gas bubble growing in an oil-refrigerant solution subjected to uniform and isothermal decompression. The model considered an elementary cell (EC) formed by a bubble surrounded by a liquid layer containing a finite amount of dissolved refrigerant. The pressure reduction in the liquid phase provokes an imbalance between the initial refrigerant concentration in the liquid layer and the equilibrium concentration at the interface. This, in turn, triggers the refrigerant mass diffusion from the liquid layer into the bubble, resulting, together with the expansion of the gas, in the bubble growth. After a certain period of time, the bubble tends to reach a stable radius as the decompression stops and the amount of refrigerant in the liquid layer decreases toward a new equilibrium condition. The system of coupled non-linear governing equations was solved numerically by the finite difference method to calculate the bubble internal pressure, the bubble growth rate and the refrigerant concentration profile in the liquid layer.

The numerical results showed that, in general terms, the bubble growth process can be divided into three distinct periods: a first period, of slow growth rate at the initial instants due to the opposing effect of the interfacial tension force, a second period, of rapid bubble expansion followed by a third period characterized by stabilization of the bubble radius. During the entire growth period, the bubble interfacial tension was the predominant force against the driving force that resulted from the pressure difference between the liquid and the gas phases. Also, the effect of gas expansion inside the bubble showed to be more predominant than the refrigerant molecular diffusion effect on bubble growth rate during most part of the total growth period. The refrigerant mass fraction profiles along the liquid layer presented sharper gradients at the interface region during the initial instants. On the other hand, for the final instants, the gradient becomes smoother in the liquid layer as the amount of dissolved refrigerant is extinguished. A parametric analysis of the model showed that the bubble behavior can be affected by several parameters. An increase of the bubble initial radius implies a decrease of the bubble stable radius and of its total growth time. A large amount of dissolved refrigerant in the liquid layer decreases the time required for a complete growth of the gas phase into a stable bubble with a larger radius. Moreover, a decrease of the initial liquid layer radius limits the final radius that can be reached by the bubble, as well as the time taken to reach the final size. On the other hand, for a fixed final bubble size, increasing the liquid layer initial pressure contributes to an increase of the first period only (slow growth). An evaluation of the influence of the decompression rate (the main contribution of the present analysis, in comparison to previous works) shows that, for slower decompression rates, the total growth period tends to increase because of the delay in the bubble expansion due to the gas compressibility effect. Finally, increasing the EC temperature leads to a faster bubble growth and in a larger stable radius. This can be explained by the influence of the temperature on the mixture viscosity and on the (molecular) mass diffusivity.

Acknowledgements

The material presented in this paper is a result of a long-standing technical-scientific partnership between UFSC and Embraco. Financial support from CNPq through grant No. 573581/2008-8 (National Institute of Science and Technology in Cooling and Thermophysics) is duly acknowledged.

References

Amon, M. and C. Denson, 1984, "A Study of the Dynamics of Foam Growth: Analysis of the Growth of Closely Spaced Spherical Bubbles", *Polymer Engineering and Science*, Vol. 24, pp. 1026-1034.

Anderson, D.A., J.C. Tanehill and Pletcher, R.H., 1984, "Computational Fluid Mechanics and Heat Transfer", Hemisphere Publishing Co., Washington.

Arefmanesh, A. and Advani, S.G, 1991, "Diffusion-Induced Growth of a Gas Bubble in a Viscoelastic Fluid", *Rheologica Acta*, Vol. 30, pp. 274-283.

Arefmanesh, A., Advani, S.G., Michaelides, E.E., 1992, "An Accurate Numerical Solution for Mass Diffusion-Induced Bubble Growth in Viscous

Liquids Containing Limited Dissolved Gas", *International Journal of Heat and Mass Transfer*, Vol. 35, pp. 1711-1722.

Barbosa Jr., J.R., Lacerda, V.T. and Prata, A.T., 2004, "Prediction of Pressure Drop in Refrigerant-Lubricant Oil Flows with High Contents of Oil and Refrigerant Outgassing in Small Diameter Tubes", *Int. Journal of Refrigeration*, Vol. 27, No. 2, pp. 129-139.

Becerra, E.C.V., 2003, "Simulação de um Compressor Hermético Alternativo Operando em Regime Transiente", D. Eng. Thesis (in Portuguese), PUC-Rio.

Bird, R.B., Stewart, W.E. and Lightfoot, E.N., 2002, "Transport Phenomena", 2nd Ed., Wiley, NY.

Brennen, C.E., 1995, "Cavitation and Bubble Dynamics", Oxford University Press, Oxford.

Carey, V.P., 1992, "Liquid-Vapour Phase Change Phenomena: An Introduction to the Thermophysics of Vaporization Processes in Heat Transfer Equipment", Hemisphere Publishing Corporation

Castro, H.O.S., Gasche, J.L. and Conti, W.P., 2004, "Foam Flow of Oil-Refrigerant R134a Mixture in a Small Diameter Tube" Proc. of the 10th Int. Refrigeration and Air Conditioning Conference at Purdue, Purdue, USA.

Castro, H.O.S., Gasche, J.L. and Prata, A.T., 2009, "Pressure Drop Correlation for Oil-Refrigerant R134a Mixture Flashing Flow in a Small Diameter Tube", *International Journal of Refrigeration*, Vol. 32, pp. 421-429.

Cho, J.R. and Moon, S.J., 2003, "A Numerical Analysis of the Interaction Between the Piston Oil Film and the Component Deformation in a Reciprocating Compressor", *Tribology International*, Vol. 38, pp. 459-468.

Conde, M.R., 1996, "Estimation of Thermophysical Properties of Lubricating Oil and their Solutions with Refrigerants: An Appraisal of Existing Methods", *Applied Thermal Engineering*, Vol. 16, No. 1, pp. 51-61.

Couto, P.R.C., 2007, "Análise de Mancais Radiais Hidrodinâmicos com Aplicação em Compressores Herméticos de Refrigeração", D. Eng. Thesis (in Portuguese), Federal University of Santa Catarina.

Dias, J.P. and Gasche, J.L., 2006, "Computational Simulation of the Oil-R134a Mixture Two-Phase Flow with Foam Formation in a Circular Cross Section Tube", Proc. of ECI Int. Conference on Boiling Heat Transfer, Spoleto, Italy.

Grando, F.P. and Prata, A.T., 2003, "Computational Modeling of Oil-Refrigerant Two-Phase Flow with Foam Formation in Straight Horizontal Pipes", Proc. of the 2nd HEFAT, Zambia.

Grando, F.P., Priest, M. and Prata, A.T., 2006a, "Lubrication in Refrigeration Systems: Numerical Model for Piston Dynamics Considering Oil-Refrigerant Interaction", Proc. of IMechE Part J: *Journal of Engineering Tribology*, Vol. 220, pp. 245-258.

Grando, F.P., Priest, M. and Prata, A.T., 2006b, "A Two-Phase Flow Approach to Cavitation Modeling in Journal Bearings", *Tribology Letters*, Vol. 21, No. 3, pp. 233-244.

Hayduk, W. and Minhas, B. S., 1982, "Correlations for Prediction of Molecular Diffusivities in Liquids", *The Canadian Journal of Chemical Engineering*, Vol. 60, pp. 295-299.

Joshi, K., Lee, J.G., Shafi, M.A. and Flumerfelt, R.A., 1998, "Prediction of Cellular Structure in Free Expansion of Viscoelastic Media", *Journal of Applied Polymer Science*, Vol. 67, pp. 1353-1368.

Lacerda, V.T., Prata, A.T. and Fagotti, F., 2000, "Experimental Characterization of Oil-Refrigerant Two-Phase Flow", Proc. of the ASME – Advanced Energy Systems Division, Vol. 40, pp. 101-109.

McLinden, M.O., Klein, S.A., Lemmon, E.W. and Peskin, A.P., 1998, "Thermodynamic and Transport Properties of Refrigerants and Refrigerants Mixtures", NIST Standard Reference Database 23, REFPROP 6.0.

Prata, A.T., Fernandes, J.R.S. and Fagotti, F., 2000, "Dynamic Analysis of Piston Secondary Motion for Small Reciprocating Compressors", Transactions of the ASME – *Journal of Tribology*, Vol. 122, pp. 752-760.

Proussevitch, A.A., Sahagian, D.L. and Anderson, A.T., 1993, "Dynamics of Diffusive Bubble Growth in Magmas: Isothermal Case", *Journal of Geophysical Research*, Vol. 98, pp. 22283-22307.

Proussevitch, A.A. and Sahagian, D.L., 1996, "Dynamics of Coupled Diffusive and Decompressive Bubble Growth in Magmatic Systems", *Journal of Geophysical Research*, Vol. 101, pp. 17447-17455.

Rigola, J., Pérez-Segarra, C.D. and Oliva, A., 2003, "Numerical Simulation of the Leakage Through the Radial Clearance Between Piston and Cylinder in Hermetic Reciprocating Compressors", Proc. of the Int. Conference on Compressor and their Systems, London, UK, pp. 313-321.

Sprow, F.B. and Prausnitz, J.M., 1966, "Surface Tension of Simple Liquid Mixtures", *Transactions of Faraday Society*, Vol. 62, pp. 1105-1111.

Street, J.R., Fricke, A.L. and Reiss, L.P., 1971, "Dynamics of Phase Growth in Viscous, non-Newtonian Liquids – Initial Stages of Growth", *Industrial and Engineering Chemistry Fundamentals*, Vol. 10, pp. 54-64.

Yanagisawa, T., Shimizu, T., Fukuta, M., 1991, "Foaming Characteristics of an Oil-Refrigerant Mixture", *International Journal of Refrigeration*, Vol. 14, pp. 132-136.

Appendix: Properties of the Oil-Refrigerant Mixture

Solubility

The solubility of refrigerant HFC-134a in polyol ester oil ISO VG10 was adjusted from data provided by the oil manufacturer as a function of the pressure, p, and the temperature T,

$$w_{sat} = \frac{a_1 + b_1 p + c_1 T + d_1 p^2 + e_1 T^2 + f_1 Tp}{a_2 + b_2 p + c_2 T + d_2 p^2 + e_2 T^2 + f_2 Tp} \tag{A.1}$$

where the coefficients are: a_1 = 0.68247268; b_1 = 0.0700619; c_1 = 0.06991081; d_1 = -0.00012087; e_1 = -0.00171566; f_1 = 0.00241240; a_2 = 1; b_2 = -0.00313147; c_2 = 0.05031545; d_2 = $1.05413714 \times 10^{-6}$; e_2 = 0.00136449; f_2 = $-6.40745705 \times 10^{-5}$. This correlation is valid for the ranges $0 < p < 100$ kPa and $0 < T < 100$°C.

Density

The density of the mixture HFC134a- ISO VG10 ester oil is calculated using the ideal mixture hypothesis (i.e., additive volumes). Thus, the density can be calculated by

$$\rho_L = \frac{\rho_{oil}}{1 + w_r \left(\frac{\rho_{oil}}{\rho_r} - 1 \right)} \tag{A.2}$$

where w_r is the refrigerant mass fraction in the mixture, and ρ_{oil} and ρ_r are the oil and liquid refrigerant densities, respectively.

Dynamic viscosity

The correlation for the dynamic viscosity of the liquid mixture composed of refrigerant HFC-134a and ISO VG10 ester oil was also obtained from data fitting provided by the oil manufacturer as follows:

$$\mu_L = 1.0 \times 10^{-6} \rho_L \frac{m_1 + n_1 T + o_1 w_r + p_1 T^2 + q_1 w_r^2 + r_1 T w_r}{m_2 + n_2 T + o_2 w_r + p_2 T^2 + q_2 w_r^2 + r_2 T w_r} \tag{A.3}$$

where w_r is the refrigerant mass fraction, T is the temperature and the coefficients are: m_1 = 38.31853120; n_1 = 0.03581164; o_1 = −0.55465145; p_1 = $-6.02449153 \times 10^{-5}$; q_1 = $7.67717272 \times 10^{-4}$; r_1 = $-2.82836964 \times 10^{-4}$; m_2 = 1; n_2 = 0.05188487; o_2 = 0.02747679; p_2 = $9.61400978 \times 10^{-4}$; q_2 = $4.40945724 \times 10^{-4}$; r_2 = $1.10699073 \times 10^{-3}$. The intervals in which the correlation is valid are $0 < T < 100$°C and $0 < w_r < 1$.

Interfacial tension

For the interfacial tension, Conde (1996) suggests the use of a simplified version of a correlation proposed by Sprow and Prausnitz (1966) for binary mixtures of non-polar fluids given by

$$\sigma = \left(1 - \psi_{r,i}\right)\sigma_{oil} + \psi_{r,i}\sigma_{lr} - \frac{A}{2RT}\left(\sigma_{oil} - \sigma_{lr}\right)^2 \psi_{r,i}\left(1 - \psi_{r,i}\right) \tag{A.4}$$

where σ_{oil} and σ_{lr} are the oil and the liquid refrigerant interfacial tensions, respectively. $\psi_{r,i}$ is the refrigerant mole fraction at the bubble interface, T is the absolute temperature, R is the universal gas constant (8314.1 J/mol.K) and A is the molar partial area calculated by

$$A = \frac{1}{2}\left[\left(\frac{M_r}{\rho_{lr}}\right)^{2/3} + \left(\frac{M_{oil}}{\rho_{oil}}\right)^{2/3}\right] N_0^{1/3} \tag{A.5}$$

where M_r and M_{oil} are the refrigerant and oil molecular weight and N_0 is the Avogadro number (6.023×10^{26} kmol^{-1}).

Mass diffusivity of the refrigerant in the liquid mixture

The mass diffusivity of the refrigerant in the liquid mixture is calculated using a semi-empirical correlation proposed by Hayduk and Minhas (1982) for non-aqueous binary solutions, assuming infinite dilution of the refrigerant. Thus,

$$D = 1.55 \times 10^{-8} \frac{\tilde{v}_{oil}^{0.27}}{\tilde{v}_{lr}^{0.42}} \frac{T^{1.29}}{\mu_{oil}^{0.92}} \frac{\sigma_{oil}^{0.125}}{\sigma_{lr}^{0.105}} \tag{A.6}$$

where D is the mass diffusivity at infinite dilution [cm^2/s], $\tilde{v}_{oil}$ and $\tilde{v}_{lr}$ are the oil and liquid refrigerant molar volumes [cm^3/mol] at the oil and liquid refrigerant normal boiling temperatures, respectively, T is the mixture absolute temperature, μ_{oil} is the oil dynamic viscosity [cP], and σ_{oil} and σ_{lr} are the oil and liquid refrigerant interfacial tensions [dyn/cm].